phys. stat. sol. (a) **173**, 495 (1999)

Subject classification: 77.80.Dj; 61.16.Bg; S10.15

Imaging of 180° Ferroelectric Domains in $LiTaO_3$ by Means of Scanning Electron Microscopy

S. ZHU[1]) and W. CAO

Materials Research Laboratory, The Pennsylvania State University, University Park, Pennsylvania 16802, USA

(Received February 19, 1999)

The 180° ferroelectric domains, engineered through field poling in single crystalline $LiTaO_3$ were directly observed by means of scanning electron microscopy (SEM) on its polished polar surfaces without metal coating. Two kinds of domain images, the brightness-contrast image and topographic-boundary image, were found with slow scan rate under the condition of a cathode voltage of $V_0 = 3$ to 5 kV and a probing beam current of $I_b = (4 \text{ to } 20) \times 10^{-11}$A. They appeared at the initial and subsequent frames of scanning, respectively. The formation of these two kinds of images is explained as pyroelectric and piezoelectric effects which originated from the beam electron heating and the charge accumulation on the top surface of a $LiTaO_3$ crystal.

1. Introduction

The study of domain microstructures becomes increasingly important for materials engineering. Therefore, visualization of domains has gained broad interests in both physics and materials science communities. Since the 1980's, scanning electron microscopy (SEM) has been used for the observation of ferroelectric domain structures by Le Bihan, Sogr, and others [1 to 3]. Some useful ferroelectric crystals, such as $BaTiO_3$, $LiNbO_3$ and $KTiOPO_4$, have been studied by using this method [4 to 6]. For most ferroelectric crystals, the secondary electron emission yield is close to one under the condition of a probing beam electron energy $E \approx 1$ to 5 keV. Therefore, there is no severe charge accumulation on the surface of an insulating sample.

$LiTaO_3$ is also an important ferroelectric crystal possessing excellent optical and acoustic properties [7]. The 180° engineered domains in the crystal have been used for the generation of second and third harmonics of laser radiation by quasi-phase-matching, and the excitation and reception of high frequency acoustic wave [8 to 10]. The domain structure in a poled $LiTaO_3$ sample can be evaluated by optical microscopy on its etched surface. In order to eliminate the damage of etching in the study of domain configuration, it is desirable to develop new convenient nondestructive methods for the observation of engineered domain patterns on an unprepared polar surface of a $LiTaO_3$ crystal.

Recently, we have successfully observed a 180° domain contrast by using the environment scanning electron microscopy (ESEM) technique [11]. The ESEM observation is performed under finite atmosphere pressure. Up to now, there are no reports on characterizing the domain structure of $LiTaO_3$ using conventional SEM. This paper reports

[1]) Permanent address: National Laboratory of Solid State Microstructures and Physics Department, Nanjing University, Nanjing 210093, People's Republic of China.

our SEM results and analyzes the interesting physical principles associated with the images.

In conventional SEM, the sample is put in a high vacuum chamber with a pressure $p < 10^{-6}$ Torr. Therefore, the observation can only be performed under the conditions of a low acceleration voltage and a small beam current in order to avoid severe charge accumulation on the insulating surface of the sample. Two kinds of domain images of $LiTaO_3$ were found in our SEM observation: brightness-contrast images and domain-boundary images. They appeared at the initial and subsequent frames of scanning, respectively.

2. Experimental Conditions

The probed samples with 180° anti-parallel domains were fabricated by using pulse-field poling on a single domain $LiTaO_3$ crystal at room temperature [12]. Under different electrodes, i.e. stripe and plane electrodes, two types of domain morphology were produced exhibiting stripe and triangular shapes, respectively. The samples were ≈0.5 mm thick with a pair of parallel polar surfaces. The poled samples were first etched. Some inverted domains with triangular shape or stripe shape on the $-c$ and $+c$ faces were confirmed by optical microscopy. Afterwards, the etched surfaces were re-polished in order to remove the topographic domain patterns and the samples were transferred into the SEM sample chamber. The bottom surface of the sample was loosely fixed to a conducting holder and the probing beam current I_b was directed towards the surface. The conducting sample holder was connected to the ground as shown in Fig. 1. The SEM investigations were performed with a scan rate of 8 to 20 s per frame by using a JEOL JSM-6300 scanning electron microscope in the secondary electron emission mode. The experimental conditions are as follows: chamber pressure $p < 10^{-6}$ Torr, probe current $I_b = 4$ to 20×10^{-11} A, and a cathode voltage of $V_0 = 3$ to 5 kV. The small probe current and the low voltage ensure a longer effective observation time.

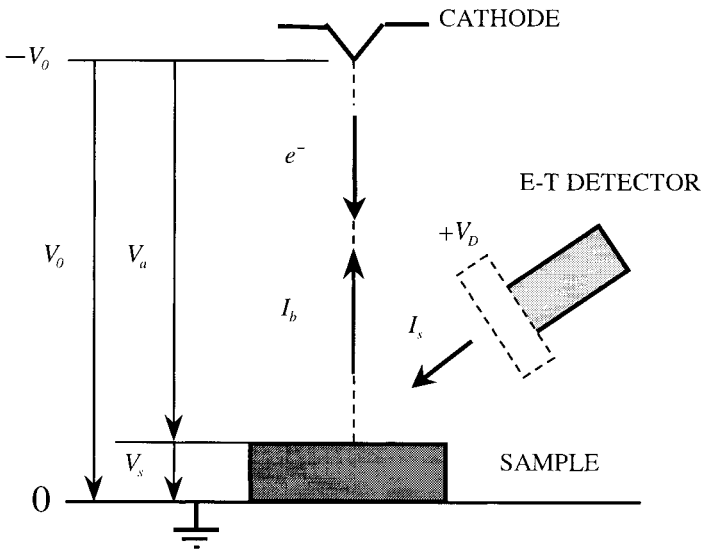

Fig. 1. Definition of the electrical potential levels of the experimental set-up

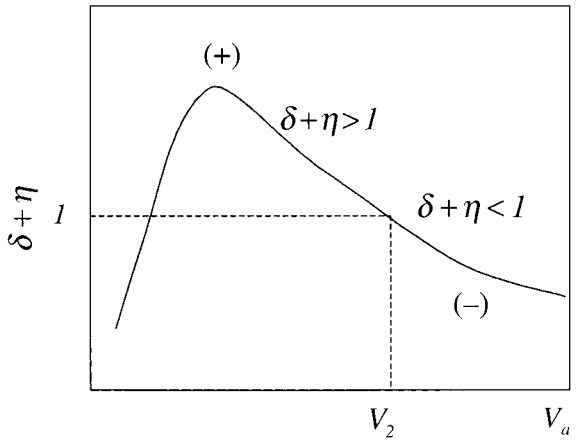

Fig. 2. Sum of the secondary and backscattered electron yield versus the effective acceleration voltage V_a of the probing beam electrons for an insulating crystal

When the primary probing beam scans the surface of the sample, the irradiated surface emits secondary and backscattered electrons. The total emitted electron coefficient $\delta + \eta$ as a function of the acceleration voltage V_a of the probing beam electrons is shown in Fig. 2, where δ and η are the yields of secondary and the backscattered electrons of the sample, respectively, and V_2 is the voltage at the equilibrium point at which the sum of the emitted electron coefficient is unity, $\delta + \eta = 1$. If the cathode voltage V_0 can be set to $V_0 = V_2$, the charges directed to the sample by the probing beam would be the same as the totally emitted charges. Thus, no net charge accumulation would occur on the top surface of the sample. If the cathode voltage V_0 is set to be greater than V_2, we obtain the condition of $\delta + \eta < 1$, which means that the sample is charged negatively that produces a negative voltage V_s across the sample. The acceleration voltage $V_a = V_0 - V_s$ will continue to increase until $V_a = V_2$. If the cathode voltage can be set to $V_0 < V_2$, more electrons are emitted and the sample will be charged positively until $V_a = V_0 + V_s = V_2$. With the approximation of a parallel plate capacitor, the electrical potential of the top surface can be written as $V_s = (ql)/(\varepsilon\varepsilon_0 a^2)$, where q, l and a are the surface charge, the sample thickness and the beam radius, respectively, while ε and ε_0 are the relative dielectric constant and free space permittivity, respectively. When $\delta + \eta \neq 1$, the effective potential from the cathode to the sample surface V_a is equal to $V_0 + |V_s|$ for $V_s < 0$ and $V_0 - |V_s|$ for $V_s > 0$ [13,14]. In our experimental conditions, the cathode voltage was set to $V_0 > V_2$, based on the fact that the sample surface was negatively charged during the scan.

3. Results and Discussion

Two kinds of SEM contrast images were obtained in our experiments. The first was a brightness-contrast image between the positive and negative domains, and the second was a domain-boundary image. The brightness contrast was shown only at the initial frame of probing electron beam scanning. The image of positive domains was brighter than that of the negative domains as shown in Fig. 3. This means that the secondary electron emission yield from the surface of positive domains is larger than that from the surface of negative domains. In the subsequent frames, the brightness contrast disap-

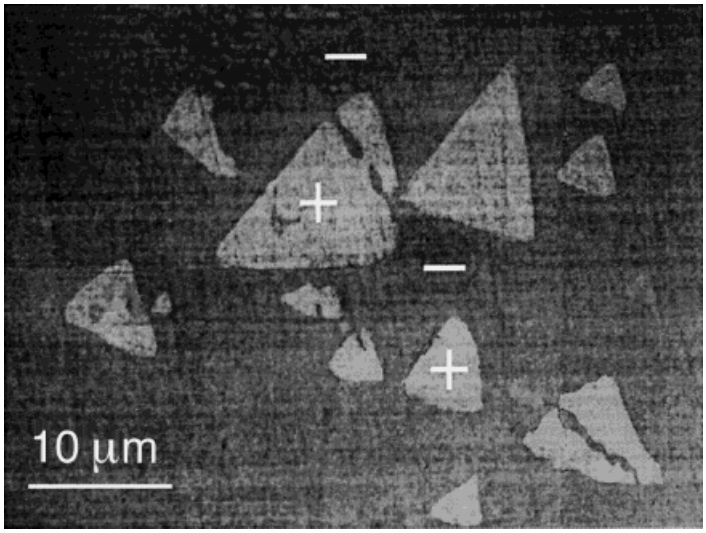

Fig. 3. Domain contrast on the $-c$ polar surface of a $LiTaO_3$ single crystalline surface at the initial scanning frame. The triangular positive domains surrounded by the negative domains are brighter

pears while the domain boundary contrast begins to appear. Fig. 4 reveals a topographic image with the higher lying surface to be the positive domains. The topographic origin of the image can be seen from the shadowing effect in Fig. 4. Some authors also reported similar results in their SEM observations of KTP [15]. These two kinds of contrasts can be of different physical origin as analyzed in more detail below.

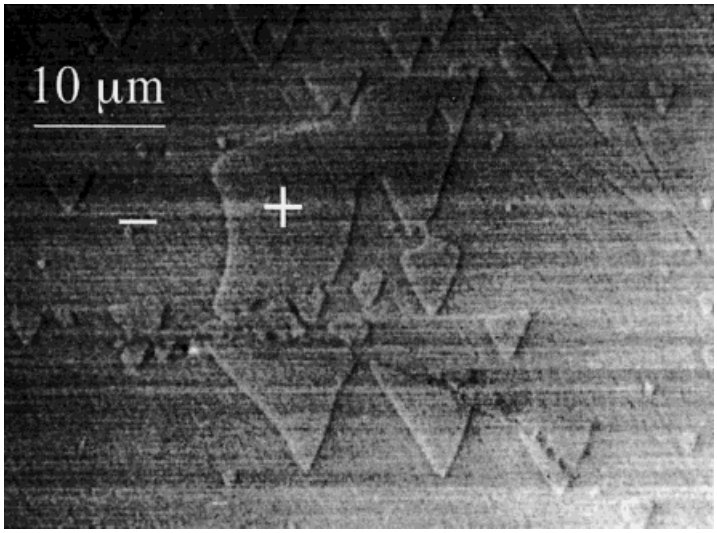

Fig. 4. In the subsequent frames, only a boundary contrast can be observed on the polar surface of the $LiTaO_3$ sample

3.1 Pyroelectric imaging

Single crystalline $LiTaO_3$ is a ferroelectric material revealing strong pyroelectric and piezoelectric effects. These effects allow secondary-electron emission from the opposite polar surfaces or their boundaries to have different yield rates which produce domain images.

According to our experimental conditions and the material parameters of $LiTaO_3$, we can roughly estimate the influence of these effects on the parameters of the secondary-electron and backscattered-electron yields, δ and η, respectively. The average energy per incident electron is $E_a = eV_a$ before they hit the sample. A portion of this energy is used to excite the secondary and backscattered electrons, while the rest of this energy is absorbed by the sample and is converted into heat. Since, the thermal conductivity of the sample is finite, there will be some temperature difference ΔT between the irradiated region and the rest of the sample. This temperature rise can be estimated by using the following formula:

$$\Delta T = \frac{t_d\{I_b(E_a - \delta\bar{E}_s - \eta\bar{E}_b)/e - L\}}{\nu\varrho c_p} \tag{1}$$

where I_b is the probe current, $e = 1.60 \times 10^{-19}$ C is the basic charge unit, $\nu = \pi a^2 h$ is the irradiated volume, h is the average penetration depth of the electron, a is the beam radius, c_p is the heat capacity per unit volume, ϱ is the density of crystal, $\bar{E}_s$ and $\bar{E}_b$ are the averaged energies of secondary and backscattered electrons. The dwell time t_d of the probing beam can be evaluated from its line scan length and line scan time. In Eq. (1), the product $t_d I_b E_a/e$ is the incident energy of probing beam electrons. If this energy is totally converted into heat, the temperature rise in the irradiated local region for a $LiTaO_3$ crystal $-\varrho = 7.456\ \mathrm{g\ cm^{-3}}$ [16] and $c_p = 0.424\ \mathrm{J\ g^{-1}\ K^{-1}}$ [17] – could be near 100 K. However, a real temperature increase is much lower than this estimated value because two factors prevent the local temperature rise. In Eq. (1), $t_d I_b(\delta\bar{E}_s + \eta\bar{E}_b)/e$ represents the energy carried away by backscattered and secondary electrons, and L is the energy loss related to the thermal conductions. According to Ref. [18], a temperature rise of a few degrees Celsius was determined for some bulk samples with a typical SEM probing beam current of $I_b = 1 \times 10^{-9}$ A [18]. In our case, the beam current was smaller but the scan rate was slower. Thus, it is expected that an increase in temperature of the same order of magnitude compared to the reported values occurred in the irradiated local region. This rise in temperature can generat a pyroelectric potential on the sample surface given by

$$U_{\mathrm{pyro}} = \frac{\varkappa\,\Delta T h}{\varepsilon_0 \varepsilon}\,, \tag{2}$$

where $\varkappa$ is the pyroelectric coefficient of the sample. For single crystalline $LiTaO_3$ [17], $\varkappa = -17.6 \times 10^{-5}\ \mathrm{CK^{-1}\ m^{-2}}$ and $\varepsilon = 43.4$. Assuming a small local rise in temperature of $\Delta T \approx 3$ K, the generated surface potential will be $U_{\mathrm{pyro}} = -2.5$ V (+2.5 V) for the positive (negative) domains. Therefore, the pyroelectric potential difference ΔU_{pyro} between the positive and negative domains can amount to 5.0 V. This potential difference is large enough to produce a potential contrast on the surfaces of the positive and negative domains because secondary electrons are low in energy (less than 10 eV) making them sensitive to the effects of surface potential and the electric field gradients. If

$U_{\text{pyro}} = +2.5\,\text{V}$ for the negative domains, the secondary electrons with energies less than 2.5 eV will not escape the sample. Thus, a smaller amount of electrons will be detected by the Everhart-Tornley detector. On the other hand, the thermally induced bias of -2.5 V for the positive domains – as calculated above – will act as a booster for the escape of secondary electrons and, hence, a larger amount of electrons will arrive at the detector. Experimentally, a higher yield of the secondary electrons was observed for surfaces of positive domains making them brighter which is consistent with our analysis. According to the above discussions, it is obvious that the contrast resulting from the pyroelectric effect is a reflection of electrical potential contrast [19]. We expect that the same effect can be produced by applying a pressure to a multi-domain single crystalline sample since the piezoelectric effect induces an electric potential difference between the end faces of the positive and the negative domains.

$LiTaO_3$ is a good insulator with a very small electrical conductivity ($\sigma < 10^{-11}\,\Omega^{-1}\,\text{m}^{-1}$) [20]. In the case that the cathode voltage $V_0 > V_2$ and the total emitted electron coefficient $\delta + \eta < 1$, the electrons tend to accumulate on the irradiated surface, producing an additional electric field in the interior of the sample. In our experiment (20 s/frame), the dwell time t_{d} of the probeing beam is approximately 10^{-5} s, therefore, the incident charge density per frame is estimated to be 2×10^{-5} C/cm^2. The effective charge density for the surface build up was much smaller because a significant fraction of the charge was scattered and emitted in the form of secondary electrons. These accumulated charges can be dissipated through the Maxwell relaxation process with a typical relaxation time of $\tau_{\text{m}} = \varepsilon\varepsilon_0/\sigma$. For a $LiTaO_3$ crystal, the relaxation time is $\tau_{\text{m}} > 30$ s. Therefore, the accumulated charges cannot be sufficiently relaxed within the dwell time t_{d}. There are still remaining charges on the surface from the previous scan even after the frame interval time t_{I} ($\approx$20 s). This charge accumulation will cause the reduction of the effective acceleration potential V_{a} between the sample and the cathode causing reduction of the velocity of the injected electrons. The situation will continuously accompany the scan process until the condition $\delta + \eta = 1$ is reached, at which time, the total charges on the sample surface reach a dynamical equilibrium.

Before the dynamic equilibrium is reached, the amount of surface charges is time-dependent and follows the simple rule of $q = q_0(1 - \text{e}^{-t/\tau})$, where q_0 is the surface charge at equilibrium, t is the observation time, and τ is the effective relaxation time. This time τ depends on the conductivity of the sample, the voltage and the current of the probing beam, the quality of vacuum in the chamber, and so on. Thus, the surface potential V_{s} can be written as

$$V_{\text{s}} = (V_0 - V_2)\,(1 - \text{e}^{-t/\tau})\,. \tag{3}$$

The average energy of an incident electron becomes

$$E_{\text{a}} = e(V_0 - V_{\text{s}}) = eV_2 + e(V_0 - V_2)\,\text{e}^{-t/\tau}\,. \tag{4}$$

When the observation time $t \gg \tau$, the average energy E_{a} approaches eV_2. Equation (4) indicates that the energy of the probing beam is a function of the observation time t. At the initial stage of scan, $V_{\text{s}} \approx 0$, $E_{\text{a}} \approx eV_0$. According to Eqs. (1), (2), (3), and (4), the resulting surface pyroelectric potential can be estimated as

$$U_{\text{pyro}} = \frac{\varkappa I_{\text{b}} t_{\text{d}}[V_2 + (V_0 - V_2)\,\text{e}^{-t/\tau} - L]}{\varepsilon_0 \varepsilon \pi a^2 c_p \varrho}\,, \tag{5}$$

where L represents the total energy loss as in Eq. (1). The pyroelectric potential on the $LiTaO_3$ surface will decrease monotonously with time during the scan process. The surface potential V_s of the positive and negative domains will differ by $2U_{pyro}$. When the observation time is short, i.e. $t \ll \tau$ the surface potential $V_s \approx U_{pyro}$ and the dominant effect producing the image is the pyroelectric potential. On the other hand, when $t \gg \tau$, $V_s \gg U_{pyro}$ and the potential difference between the positive and negative domains becomes negligible. The pyroelectric image fades away rapidly with the increase of V_s. Experimentally, the pyroelectric domain contrast can only be observed unambiguously in the first frame of the scan.

3.2 Piezoelectric imaging

The piezoelectric effect becomes more and more visible with the build up of the surface potential V_s, which leads to a topographic domain pattern. The electric field induced by the surface charge accumulation along the thickness direction is $E = V_s/l$, where l is the thickness of the sample, which induces an elastic strain of $S = \Delta l/l = d_{33}\, E$ in the poling direction through the converse piezoelectric effect. For $LiTaO_3$, $d_{33} = 9.2 \times 10^{-12}\,\mathrm{CN}^{-1}$ [21]. Thus, the surface displacement Δl is given by

$$\Delta l = d_{33} V_s = d_{33}(V_0 - V_2)\,(1 - \mathrm{e}^{-t/\tau})\,. \tag{6}$$

When $t \gg \tau$ and $V_s \approx 3$ kV, $\Delta l \approx \pm 0.03$ μm. For positive domains, the electric field vector **E** is parallel to the polarization vector **P** so that the displacement Δl is positive. The electric field vector **E** is anti-parallel to **P** for the negative domains resulting in a negative displacement Δl. Since the bottom side of the sample surface is only weakly fixed to the sample holder and free to deform, the surface displacement difference between the positive and negative domain on the top surface is only 0.03 μm. The domain-boundary contrast is a topographic one, which originates from the high surface potential built by the beam deposited charge accumulation. In Fig. 4 the boundaries between

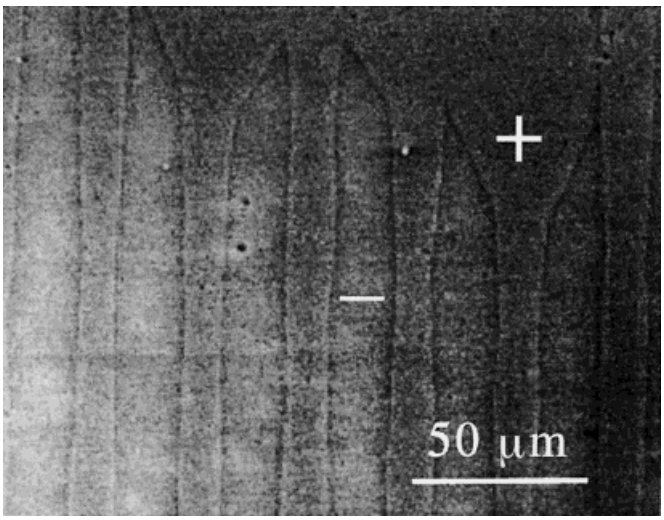

Fig. 5. Domain image of a periodically poled $LiTaO_3$ sample

the positive and negative domains indeed show sub-micron steps. We also observe the boundary contrast for lower values of V_0 ($V_0 \approx 3$ kV); the image was the same except of a shallower boundary step as expected. This fact revealed that the equilibrium potential V_2 of the secondary electron emission in $LiTaO_3$ is lower than 3 kV. We used the SEM technique to check $LiTaO_3$ samples poled periodically and quasi-periodically and satisfactory images were obtained in both cases. Fig. 5 is an image of a periodic domain structure of a $LiTaO_3$ surface.

4. Conclusions

In conclusion, the two different kinds of domain contrast images, i.e., the brightness contrast and the domain-boundary contrast, were observed on the polar single crystalline surface of $LiTaO_3$ by using conventional SEM. At the initial frame, the pyroelectric potential leads to different secondary-electron yields from the positive and the negative domain surfaces and, thus, forming a brightness contrast and produced a domain image. The topographic domain patterns were produced by the piezoelectric effect in subsequent scan frames with the increase of the charge accumulation at the polar sample surface due to the insulating nature of the sample. Hence, a domain boundary image was observed. Our results showed that the 180° anti-parallel engineering domains of single crystalline $LiTaO_3$ surfaces can be imaged by the conventional SEM under the conditions of non-surface etching and non-coating. This establishes a nondestructive method for the observation of the engineering domain structures of single crystalline $LiTaO_3$ samples.

Acknowledgement This research was sponsored by the U.S. National Science Foundation Grant # DMS-9704714.

References

[1] R. LE BIHAN, Ferroelectrics **97**, 19 (1989).
[2] A. A. SOGR and I. B. KOPYLOVA, Ferroelectrics **191**, 193 (1997).
[3] A. SKLIAR et al., Ferroelectrics **191**, 187 (1997).
[4] G. ROSENMAN, A. SKLIAR, Y. LAREAH et al., J. Appl. Phys. **80**, 7166 (1996).
[5] D. V. ROSHCHUPKIN and M. BRUNEL, Scanning Microscopy **7**, 543 (1993).
[6] T. OZAKI, K. FUJII, and S. AOYAGI, J. Appl. Phys. **80**, 1697 (1996).
[7] Y. XU, Ferroelectric Materials and Their Applications, North-Holland Publ. Co., New York 1991.
[8] S. N. ZHU, Y. Y. ZHU et al., Phys. Rev. Lett. **78**, 2752 (1997).
[9] S. N. ZHU, Y. Y. ZHU, and N. B. MING, Science **278**, 843 (1997).
[10] Y. F. CHEN, S. N. ZHU, Y. Y. ZHU, and N. B. MING, Appl. Phys. Lett. **70**, 592 (1997).
[11] S. N. ZHU and W. CAO, Phys. Rev. Lett. **79**, 2558 (1997).
[12] S. N. ZHU, Y. Y. ZHU et al., J. Appl. Phys. **77**, 5481 (1995).
[13] R. LE BIHAN and M. MAUSSION, Rev. Phys. Appl. **9**, 427 (1974).
[14] P. R. THORNTON, Scanning Electron Microscopy, Chapman & Hall, London 1968.
[15] G. ROSENMAN et al., Phys. Rev. B **54**, 6222 (1996).
[16] S. C. ABRAHAMS and S. C. BERNSTEIN, J. Phys. Chem. Solids **28**, 1685 (1967).
[17] H. P. BEERMAN, Infrared Phys. **15**, 225 (1975).
[18] J. I. GOLDSTEIN, Scanning Electron Microscopy and X-Ray Microanalysis, Plenum Press, New York 1992.
[19] L. REIMER and G. PFEFFERKORN, Raster-Elektronen Mikrokopie, Springer-Verlag, Berlin 1973.
[20] G. I. ROZENMAN, J. S. REZ, TU. L. CHEPELEV, and N. B. ANGERT, Soviet Phys. – Tech. Phys. **26**, 234 (1981).
[21] T. YAMADA, H. IWASAKI, and N. NIIZEKI, Jpn. J. Appl. Phys. **8**, 1127 (1969).